CHAPTER 2 SATELLITE IMAGE ANALYSIS

2-1 Introduction

2-1-1 Objectives

The analysis aims to provide basic material for the selection of promising areas through the photogeologic interpretation using the LANDSAT TM images of study area. The results are analyzed and interpreted with reference to the existing geological information.

2-1-2 Study area

The study area of this phase is located in the northern part of Chile, and is located at border with Peru to the north and Bolivia to the east. This area has large areal extent from lat 17° 30′ S to lat 21° 15′ S (hereafter it is abbreviated as the study area). The study area is covered by six scenes of LANDSAT TM images.

2-1-3 Used data

(1) LANDSAT TM image

The data used was observed by LANDSAT 5 and bulk correction carried out. They were purchased from EROS Data Center of USGS through the Remote Sensing Technology Center of Japan. The observation data of each image of six scenes are shown in Table1.

When data was acquired, the available LANDSAT TM data of the object area at EROS Data Center were inquired through the Remote Sensing Technology Center of Japan, and the best data for image analysis were selected after consideration of data loss, amount of cloud cover, amount of snowfall, observation time, and etc.

The name of a representative locality of the image was adopted for the image name. The district name shown in Table2-2-1 is used in this report.

Table 2-2-1 Coordinates, Acquisition Date and Sun Elevation of TM Image of Each Area

No.	Sub-area	Name of Image	Path	Row	Acquisition Date	Sun Azimuth	Sun Elevation
1	VOLCAN TACORA	VOLCAN TACORA	002	072	1987.01.13	103.35°	51.51°
2	ARICA	ARICA	002	073	1987.01.13	101.61°	51.60°
3	SALAR DE SURIRE	SALAR DE SURIRE	001	073	1987.02.07	92.41°	49.73°
4	IQUIQUE	IQUIQUE	002	074	1987.01.13	99.84°	49.73°
5	MAMIÑA	MAMIÑA	001	074	1987.01.13	90.79°	49.54°
6	SARAL DE LLAMARA	SARAL DE LLAMARA	001	075	1987.02.07	89.21°	49.32°

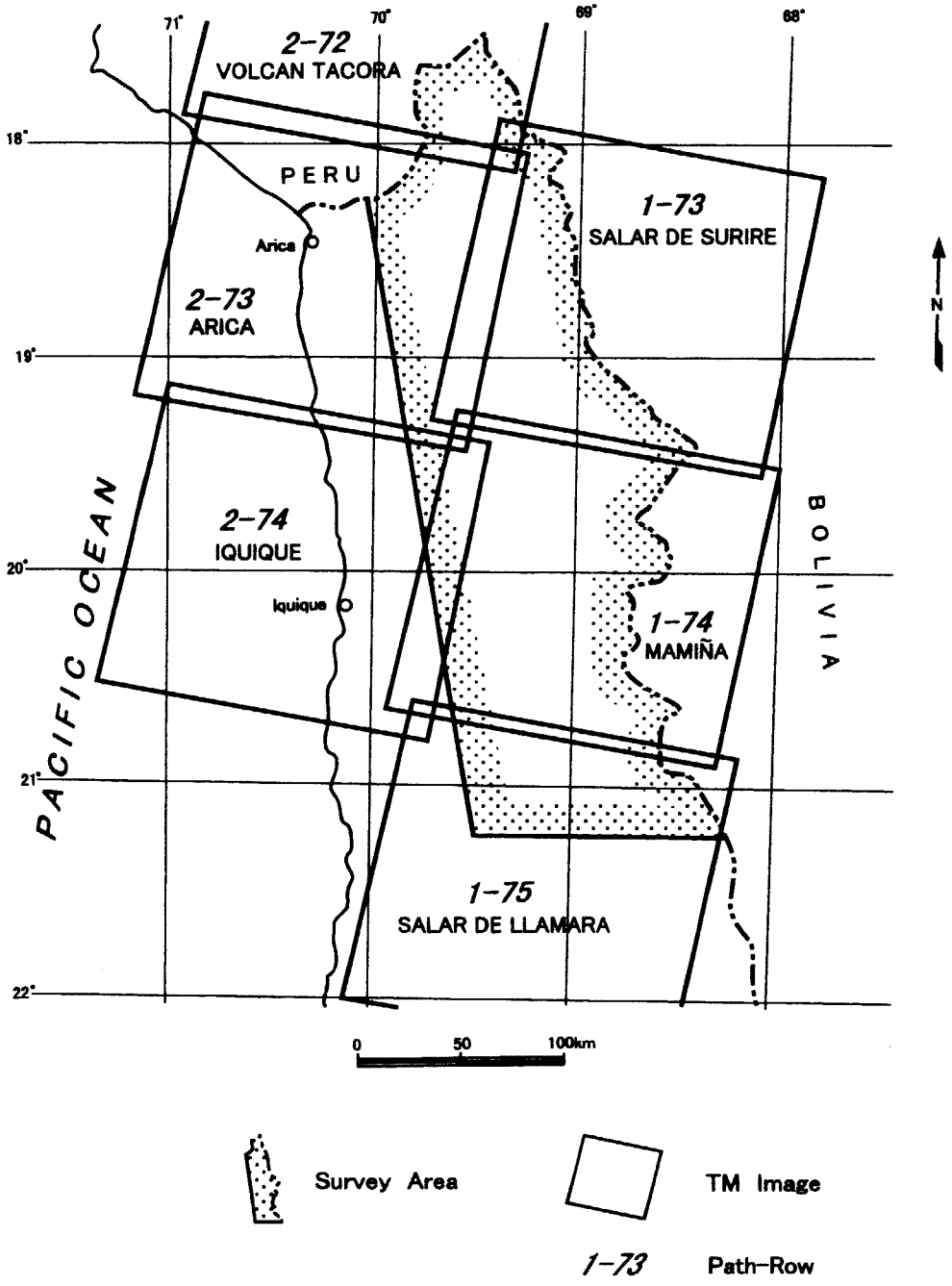

Fig. 2-2-1 Location Map of Satellite Images

2-1-4 Image processing

False color images of six scenes and ratio images and false color digital mosaic images of the whole area were made for geological and geological structure analyses and extraction of alteration zones.

False color images and ratio images were prepared so that the same lithofacies and alteration zones of different scenes would be shown by same color. Digital mosaic images of six scenes covering the whole region were prepared by combining the same bands as the false color images. The mosaic was processed so that difference of tone would not occur between adjoining images. Such process is described as follows.

(1) Preparation of false color synthesis images

To preparation the above false color synthesis images, radiometric correction which consist of incident ray value correction, atmospheric correction, and directional reflectance factor correction are necessary. The reasons for the correction and the method are described below.

(A) Necessity of radiometric correction

The LANDSAT TM sensor has a total of seven bands (four bands are in visible and infrared region, two bands are in short-wave infrared region, and one band is in thermal infrared region). Observed analog image data is converted to digital data of 256 gradation (from 0 to 255) per 1 pixel.

Brightness obtained by optical sensors such as LANDSAT TM, shows the reflection of the sun ray from visible to the short-wave infrared region. It can identify the earth's surface material by the difference of a particular spectrum reflectance of the object on earth's surface. Incident spectral radiation brightness to the sensor is the ray reflected from the earth's surface and traveled through the atmosphere. Therefore, radiation ray from the atmosphere which is called path radiance, scattering ray and scattering radiation by scattered sun ray at atmosphere which is called sky-ray besides reflectance ray are included in the radiation brightness which reaches the sensor. Therefore, when the sensor observes below by wavelength λ, the incidence spectrum radiation brightness can be approximated to the expression below.

$$L(\lambda_1, \lambda_2) = \int_{\lambda 2}^{\lambda 1} K(\lambda)[\tau a(\lambda)\{U(\lambda) + P(\lambda)\}\rho(\lambda) + b(\lambda)]d\lambda$$

$L(\lambda_1, \lambda_2)$	: Spectrum radiation brightness to sensor from wavelength λ_1 to λ_2
$K(\lambda)$	: Response characteristics of sensor
$\tau a(\lambda)$	: Transmissivity of atmosphere to reflection ray
$U(\lambda)$	: Radiation brightness of direct sun ray
$\rho(\lambda)$	: Reflectance from surface of the earth
$b(\lambda)$	: Atmospheric radiation and scattering between sensor and objects
$P(\lambda)$	: Radiation brightness of the sky ray which is the lower scattered light of the sun ray

$b(\lambda)$ is the addition factor of the brightness input to the sensor, and $U(\lambda)$, $P(\lambda)$, and $\tau a(\lambda)$ are the multiplication factors. Because the influence by these factors differ depending on the amount of steam and the amount of aerosol in the atmosphere, the spectrum radiation brightness is not the same for the same material if the observation time is different. Moreover, because the influence of these absorption ray and scattering ray has the wavelength dependency, the ratio of the band of the spectrum reflectance of a certain material is not constant in the images. Therefore, the same material will have a different tone when the images are processed by the amount of the uncorrected radiation of each band, and the material cannot be compared or be distinguished.

The radiometric correction was carried out on the following assumptions. The reason is that the image data used for present analysis were acquired at different periods, and these assumptions are necessary for showing the same material by the same tone through the entire image.

- The response characteristic of the sensor is that the output is linear-line type (y=ax) for the incident brightness.
- The transmissivity of atmosphere to the reflection light is equal in any region in one image
- Atmospheric radiation and scattering between the sensor and the object are equal in any region in one image.
- The radiation brightness of the sky ray is equal in any region in one image.

(B) Correction of incident ray value

The radiation brightness of direct incident sunray also differs by locality in a single image. In other words, when the sun is on the northern side in the Southern Hemisphere, direct

incident ray in an image increases northward, and decreases southward. Therefore, amount of the incident ray was corrected so that the azimuth of the sun would be 60° from geographic coordinate position of each pixel.

(C) Atmospheric correction

Atmospheric correction concerns $\tau a(\lambda)$ and $b(\lambda)$. The amount of obtain incident ray $\{U(\lambda)+P(\lambda)\}$ and earth's surface reflectance $\rho(\lambda)$ are necessary for this correction.

As for the correction of incident ray (b), it is required that all objects in the image are on a single plane. In reality, however, topographic relief exists and if the sun position is different, $\{U(\lambda)+P(\lambda)\}$ is different for the same point in the image different time. This $\{U(\lambda)+P(\lambda)\}$ can be corrected by using accurate DTM (Digital Terrain Model). However, this is not realistic at present because areas with accurate DTM are limited. The method we used for eliminating the topographic dependency is as follows. Take two images and use many sets of pixels of the two images corresponding to each other and statistically process the overlapping parts. Method generally used is a brightness average and standard deviation agreement method. This uses statistical amounts for the entire overlapping area. And the brightness correction value is calculated by the equation below.

$$P'_{ij}=(P_{ij}-P_{av})/\sigma_p \times \sigma_q+Q_{av}$$

P'_{ij}: Brightness conversion value
P_{ij}: Arbitrary point of brightness conversion image
P_{av}: Brightness average value of brightness conversion image
σ_p: Brightness standard deviation of brightness conversion image
Q_{av}: Brightness average value of standard image
σ_q: Brightness standard deflection of standard image

The assumption here is that material of earth's surface is similar throughout in the overlapping area, and that $\rho(\lambda)$ is equal at the times of date acquisition. In the present case, however, data were acquired at different seasons. Thus vegetation, snow cover, cloud cover, fog, drainage, and surface constructions of overlapping areas changed during the data acquisition for the two images. The brightness average and standard deviation method cannot be used, and the following method was used.

Analysis of the brightness difference between the corresponding points of the two images

was carried out. The brightness value of a standard image was shown as the horizontal axis and brightness value of corresponding image was taken as the vertical axis. Analysis was carried out for the whole overlapping area. As a result, the distribution of the corresponding points whose spectrum reflectivity $\rho(\lambda)$ changes greatly such as vegetation, shadow, snow, and cloud, become random or peculiar point group and can be identified by drawing in the scatter chart.

There is no large change in $\rho(\lambda)$ of the majority of corresponding points after eliminating the above. Point groups are distributed near a certain straight line with high correlation. Such distribution reflects the influence of the difference of $\{U(\lambda)+P(\lambda)\}$ by relief energy. Then, these are approximated by least-squares, and the influence by topographic features is removed.

Atmospheric correction factor by $\tau a(\lambda)$ and $b(\lambda)$ between two images can be calculated from $\{U(\lambda)+P(\lambda)\}$ obtained thus and $\rho(\lambda)$ corrected by approximation.

If the observation was made the same day, it is possible to approximate to the straight line that passes the origin. This shows that transmissvity $\tau a(\lambda)$ of the atmosphere, atmospheric radiation and scattering $b(\lambda)$ between two images are equal.

If the observation day is different, approximation line can be generally shown by a straight line that does not pass through the origin (y=ax+b). This shows that neither permeability $\tau a(\lambda)$ of atmosphere, an atmospheric radiation nor scattering ray $b(\lambda)$ are equal, and this approximation line can match atmospheric permeability $\tau a(\lambda)$, atmospheric radiation, and scattering ray $b(\lambda)$ of both images.

Because the gain of the sensor of observation time is different, these paragraphs accurately reach the value to multiply $K(\lambda)$ to $\tau a(\lambda)$ and $b(\lambda)$ respectively. However, the gain of the sensor can be corrected in the lump in this technique.

Because accuracy of the atmospheric correction between the same observation days is high, an atmospheric correction of the entire six scenes was executed by the following procedures.

(a) Atmospheric correction was done for each path, and a standard image of atmospheric correction was the one at the northern most side of each path.

(b) Atmospheric correction of each image was carried out consecutively southward.

(c) Atmospheric correction between two paths was based on path (001) in the east.

The state of the atmosphere of the entire image can be matched to the state of atmosphere on the image at the northeast edge (path001/row073) by carrying out such processing.

(D) Directional reflectance factor

In complete scattering reflection bodies, reflectance of the incident vertical ray whose reflecting ray is observed vertically is defined as 1. Under such conditions, reflectance decreases gradually from 1 to 0 when the observation position gradually changes from vertical to horizontal.

The lateral view angle of the LANDSAT TM image (almost east to west) is about 16° . Therefore, when the sun light is irradiated from the right side of the image, the difference of the angle of sun-object-observer is about 16° from the right of the image to the left. In these cases, the phenomenon is the same observing complete scattering reflection bodies at different angles. It is impossible to correct each pixel because this directional reflectance differs by the material and the wavelength, and this directional reflectance depends on topographical features. However, when the eastern edge of an image is compared with the western edge, the brightness decrease about 10% on right (east) side where the angle of sun-object-observer increases (assumption; the sun irradiates ray from the eastern side of images, 90° in the azimuth, and the height 60° , there is no relief energy of the earth, the basalt of the moon is the distributed material.). Therefore when three images are joined in the E-W direction, if brightness on the western edge is taken as a standard one, the brightness decreases about 27%(=0.93) at the eastern edge. As a result, the eastern side of the image clearly becomes dark.

Thus, the change of the brightness value of the entire atmosphere-corrected image was examined by using statistics. The reason to use statistics is to exclude the influence caused by relief energy and influence of the earth's surface material. About 13,000 data is used for statistics of each row. The brightness of each pixel of the image was treated as a matrix type. And an average value and standard deviation of each line and the row were calculated. However, the acquisition beginning position of the image on the west edge was horizontally shifted because each image is a parallelogram, and acquisition position of each image was arranged to form the matrix.

The change of the average value of the breadth direction (east and west) of the image and length direction (south and north) of the image obtained by these matrix recurred by the straight line, and the direction reflection coefficient correction was made.

(E) Preparation of false color images

The brightness of all scenes are based on P001/R073 by the above correction methods. However, statistics of the LANDSAT TM image data (average value, standard deviation, and distortion degree) are different for each band, and, in general, the scattering of data is small as 20-30(256 gradation). Therefore, if this image is used without correcting, the color will not be balanced and the tone difference will be poor by small data scattering, and the image will not be suitable for interpretation.

These points were improved, and the same brightness correction was made to all scenes by using nonlinear stretch to display the radiometric correction images of all scenes appropriately. The technique used at this time has average brightness of about 115(256 gradation) (it is easy to distinguish the gradation difference of a dark area even if it is the same step difference.). This was done by nonlinear stretch so that distribution form will be close to normal distribution. The form of normal distribution was calculated so that 2.5 times standard deviation might become 115 gradation. Moreover, when statistics in the whole area was calculated, the cloud, the snow, and the waters were excluded.

The method of sharpening includes various methods, such as Laplacian, Gaussian filter or limited part sharpening. However, Gaussian filter and limited part sharpening use stretch techniques in compliance with the area to emphasize the difference with the surrounding material. As a result, it is expressed by a different tone according to the area even if the material is the same. Then, when sharpening at this time, only Laplacian filter to be not caused such a phenomenon was used.

The combination such as bands 1, 4, and 5, bands 1, 4, and 7, and bands 4, 5, and7 were examined as a band combination of false color image. It was judged unsuitable for imaging because scattering of digital value of band 1 was small partially, bands 4, 5, and7 was selected, and the image by which blue, green, and red were allocated in bands 4, 5,and 7 was made.

(F) Geometric correction

The geometric transformation into UTM coordinates of the images was done by using

prepared false color images and topographical maps (reduced scale 1/250,000). It was difficult to select high accuracy GCP(Ground Control Point) because the most accurate topographical map available was 1/250,000, and because the region consists mountains and desert where drainage is not developed and there are few landmarks. Thus, 15-20 points such as river turning point and the road intersection were selected as GCP for each image. Pseudo Affine transformation was used as interpolation, inaccurate GCP was deleted so that error of re-calculation by least-square will be within 30 pixel (about 1km). Using bi-linear method for the geometric transformation, re-sampling was done with the condition that the size of one pixel is 30m.

(2) Preparation of ratio image

(A) Concept of ratioing

LANDSAT TM observes the spectrum radiation brightness input to the sensor in seven wavelength regions (bands) in visible-middle infrared region. Radiation brightness Ni(unit mW/cm2 sr) of the ground object seen from the sensor is assumed to be expressed by the next expression.

$$N_i=(1/\pi)(H_iR_iT_iA_i)+N_{pi}$$

H : Irradiance of the sun radiation ray

R : Reflectance of the ground object

T : Transmissivity of atmosphere (vertical)

A : Coefficient determined by both the angle between earth's surface and line joining the sun & the objection on the earth, and the angle between the earth's surface object and the sensor

Np: Path radiance of atmosphere

i : Band of sensor

The spectrum characteristic can be emphasized by obtaining the ratio between two channels, because A takes a constant value regardless of the channel and it is thought that H and T take a constant value of each channel, if N_p can be presumed. That is, because the value of the ratio of the pixel where the mineral exists increases if the ratio of the channel that takes the maximum and minimum value in reflection spectrum pattern of a certain mineral is taken, the distinction with the pixel which does not exist becomes easy.

A basic idea of the ratioing is to express the range where a specific mineral is distributed in

the image emphasized by using this characteristic.

The ratioing assumes the minimum value of a digital value to be path radiance of atmosphere, obtains the value by which minimum value is subtracted from a digital value of each band, and obtains the ratio between bands of these values. To express the ratio between straps as an image, the density conversion described in the preceding clause (Preparation of false color synthesis images) is needed though the ratio (ratioing value) between bands usually takes the value of about 10 from 0. The density conversion was done by the following procedures.

The distribution of the ratioing value on the alteration zone is determined by referring to the known alteration zone described in existing geological material. A slightly wider area than this ratioing value distribution is taken, and the value of 0 is substituted for the pixel with the ratioing value that comes off from this range of distribution. If ratio operation value 0 is excluded, the image can be expressed in various densities if the density is converted, because the decentralization of the ratio operation value of the remainder becomes small compared with the decentralization of an original ratio operation value. The density conversion is done by using the following linear function.

$$G_i = a \cdot F_i + b$$

F_i: Ratioing value, G_i: Output image density value

a: Gain b: Bias

a and b are obtained from actual ratioing value distribution.

(B) Preparation of image

Hydrothermal deposits of the porphyry copper type and others are distributed in the target region, and they are accompanied by characteristics hydrothermal alteration zones. To extract these hydrothermal alteration zones from the LANDSAT TM data, it is confirmed that the ratioing of 3/1, 5/4, and 5/7 are effective on similar operations at Escondida region and the Vergua Progreso region in Chile.

The ratio operation processing images by two combinations of 5/7, 5/4, 3/1, and 5/7, 4/7, and 4/5 were compared in two districts (P001/R074 and P001/R075 to which the known alteration zone were distributed) this time. As a result, it is understood that the most effective combination to the alteration zone extraction is a ratioing image by which 5/7, 5/4,

and 3/1 are allocated in R, G, and B. The alteration is expressed in red pink and white pink in this combination. In the image processing of the district other than them, the average value of the gain and the bias which had become the best these two districts were used. In this image making, geometric correction was done by GCP used by the false color synthesis image making, and the image was put on UTM coordinates.

(3) Preparation of mosaic images

(A) Image compression and geometric transformation

To make the false color mosaic image of six scenes, the compression processing by which the image size was reduced was done. The reason is for a huge amount of data (14,000 pixels $\times$23,600 pixels $\times$ 3 bands =1 Gbyte) of image after mosaic is made when the compression processing is not done, and the amount of data exceeds a physical limitation of the film output in addition.

The radiometric correction image of each scene that has already been described was compressed by using of the geometric transformation method of changing 16 pixels (4×4) into 1 pixel by bi-linear method. Next, the correspondence point from the overlapping area of 2 images to 10-20 points was visually selected, and the geometric transformation coefficient was calculated by the Helmert's transformation that used the least-square method. When this process had been done, The large error data were deleted so that the error after re-calculation is installed within 1 pixel, and conversion coefficient of the Helmert's transformation was obtained. The geometric transformation is executed by bi-liner method.

(B) Image joining

In the image obtained at different times, the region where the tone is plainly different is caused in the joint part of two images by the shadow position, the change of material covering the earth's surface, the cloud cover and others. This clearly seen tone difference does not disturb geologic interpretation, but gives an imperfect impression of the mosaic image.

Therefore, we newly developed "drunker walk type image joining method". By this method images are connected through the regions where the tone difference is small. This technique can connect images while avoiding the regions with the cloud and shadows.

Image joining was sequentially done based on the image on the north side of each path,

and two long mosaic images of P001/R073-075 and P002/072-074 were made. Next, the corresponding points with the image on the west side is put based on the mosaic image of P001, and they are converted by the Helmert's transformation, and the image joining was done by the above technique. The size of the image by which two path connected became about 3,500 pixels ×5,900 pixels.

(C) Geometric transformation

Connected mosaic image range is within long 67-70° W and lat 16 ° 30 ´-20 ° 30 ´S. Because this range within the UTM19 belt, the mosaic was also converted geometrically into UTM coordinates as well as each image.

(4) Analytical method

The photogeologic interpretation and analysis on the satellite image are usually carried out in the following five steps:

(1) Preparation(acquisition of satellite data, orientation, collection and review of the existing information on geology and mineralization).
(2) Image data processing and generation of image preparation.
(3) Photogeologic interpretation and integrated interpretation (the integrated interpretation map is produced and compared with existing data).
(4) Field verification survey and re-interpretation based on the interpretation (3).
(5) Reporting

In this analysis, (3) and (4) were not carried out among the step s mentioned above.

The photogeologic interpretation and method of the expression are based on the following criteria.

(A) Photo-characteristics

- Tone: white, light gray, gray, bluish gray, grayish green, green, dark green, grayish purple, blown.
- Texture: fine, medium, coarse, smooth.

(B) Geomorphologic

- Drainage pattern: dendritic parallel, lattice, pinnate, with sink hole, etc.

- Drainage density: very low, low, medium, high, very high.
- Rock resistance (a level against weathering and erosion): very low, low, moderate, high, very high.
- Cross section: slope form.
- Development of bedding: well bedded, partially bedded, massive, etc.

(C) Superficial cover

- Vegetation: dense, moderate, sparse
- Cultivation: dense, moderate, sparse

Regarding the lineaments, the following criteria were employed for the identification standards:

(a) Existence of fault-scarp.
(b) Existence of fault valley.
(c) Linear arrangement of drainages.
(d) Existence of kerncol, kernbut.
(e) Linear arrangement of slope inflections.
(f) Linear arrangement of boundary of sedimentary faces.
(g) Displacement of ridge and drainage.
(h) Linear arrangement of the first-order lattice or angular drainage systems.
(i) Linear arrangement of lakes, hot springs, volcanic vents, water wells, land slides.
(j) Displacement of alluvial fans.
(k) Linear boundary of river terraces.

The above features vary in accordance with the geology, geologic structure and other factors of the area in question. However, in this analysis, many of the lineaments on the images represent the features (a), (b), (c) and (e), and partial lineaments on the images represent the feature (f), (g), (h) and (i). It is necessary to use the image of the large scale or to do stereoscopic view of spot HRV image and the aerial photograph to interpret the geographical feature.

2-2 Geological Interpretation and Analysis of Satellite Images

In this paragraph, the results of the interpretation of geology and geologic structure and extraction of alteration zones from the satellite images are described for each sub-area. At

each sub-area, the geologic units, the distribution of alteration zones, lineaments, and fold and annular structures by geololgical interpretation are described separately.

The results of the interpretation of geology and geologic structure and extraction of alteration zones at each sub-area were shown in Figures 2-2-2, 2-2-3 and Plates 1 to 5 as the photogeological interpretation map.

These results are laid out in Tables 2-2-2 to 2-2-12 with stratigraphy of the study area, which was correlated among the geological map of Chili (1/1,000,000), Arica (1/300,000), Collacagua (1/250,000), Ollagüe (1/250,000), and Calama (1/250,000).

2-2-1 Volcan Tacora sub-area

(1) Geologic units

The rocks and sediments in this sub-area are divided into six geologic units (shown in Plate 1 and Table 2-2-8). Of these units, one can be correlated with Cretaceous volcanic rocks, three with Tertiary to Quaternary volcanic rocks and two with Quaternary unconsolidated sediments.

Geologic unit K correlated with the Cretaceous volcanic rocks is distributed along the NW-SE direction, and continuously extended into the Peru.

(2) Alteration zones

In this area, 20 alteration zones, named Alteration Zones VT 001 to 020, were extracted (Plate 1 and Table 2-2-8). Among these, four altered zones (VT 015,016,017 and 020) overlap with Ar 001,002,003,004 of the ARICA Area, and two zones (VT 018,019) overlap with SS 001,002 of the SALAR DE SURIRE Area. These alteration zones trending roughly NW-SE tend to divide into two parallel zones. The zones generally show elliptic or irregular form. The largest alteration zone among them is VT 001 (4 km+α $\times$6.5 km), which is distributed near the border with the Peru and extended into the Peru. VT 013 alteration zone(3.7 km $\times$ 2.0 km) has the second largest scale by which VT 007 (3.2 km $\times$ 1.5 km) follows this in addition. These zones are distributed in the geologic unit K.

(3) Lineaments

Lineamants were extracted as shown in Plate 1 by the interpretation criteria explained in 2-1-4 (4). The solid lines in the figure are lineaments which are clear and continuous and the broken lines indicate those which are descontinuous or are not clearly shown.

Though extracted lineaments are very few in this area, the area is divided into three parts (the northern, the eastern and the western parts) regarding the distribution and the directions, and the following characteristics in each part are noted.

(i) Northern part

This part is mainly composed of Tertiary and Cretaceous volcanic rocks, and only seven lineaments were extracted in the part. Of these, three lineaments trend in NW-SE direction and two in NNW-SSE direction. These are discontinuous and 5 - 7 km long.

(ii) Eastern part

The part is mostly underlain by Cretaceous and Tertiary to Quaternary volcanic rocks. Interpreted lineaments have NW-SE and the E-W trends and are around 5 km long, and the longest one is about 8 km. NW-SE trending lineaments are noted in the vicinity of the altered zones of VT 018 and VT 019.

(iii) Western part

Lineaments in this part are the most predominant in the area and are with NW-SE and NNE-SSW trends. These are around 2-3 km long, and about 7 km is the longest. Lineaments with NW-SE and NNE-SSW trends are recognized in the vicinity of the altered zones VT 002, 006, 007 and 008.

(4) Fold structure and annular structure

(i) Fold structure

In this area, fold structure has not been interpreted in area of volcanic rocks and Quaternary sediments.

(ii) Annular structure

Annular structure was not extracted in the area.

2-2-2 Arica sub-area

(1) Geologic units

The rocks and sediments in this sub-area are divided into 13 geologic units (shown in Plate 2 and Table 2-2-9). Of these units, one can be correlated with Jurassic sedimentary rocks, two with Cretaceous to Tertiary volcanic rocks, five with Tertiary to Quaternary volcanic rocks or sedimentary rocks and four with Tertiary to Quaternary unconsolidated sediments.

Moreover, one geologic unit can be correlated to the intrusive body generated during Cretaceous to Tertiary time. Because the northeastern mountaineous part of the area was covered with the clouds, the interpretation of this part was done by the satellite image of adjoining SALAR DE SURIRE Area.

(2) Alteration zones

In the area, 20 alteration zones, named Alteration Zones Ar 001 to 020, were extracted (Plate 2 and Table 2-2-9). Among these, three altered zones (Ar 001,002 and 003) overlap with VT 015,016,017 of the VOLCAN TACORA Area north of the area , and 10 zones (Ar 007, 011, 012, 013, 014, 015, 016, 017, 018, 019, 020) overlap with SS 003, 005, 006, 007, 008, 009, 010, 011, 004, 058 of the SALAR DE SURIRE Area in the eastern vicinity of the area. In spite of each alteration zone extending in various directions, these are arranged in NNW-SSE to NW-SE direction as a whole. The alteration zones generally show elliptic or irregular form. The one with the largest scale of these zones is Ar 007 with 4.5 km×2.0 km scale and NE-SW trend, and the circumference of this zone is covered with geologic unit Tvl. Ar 014(3.5 km×2.0 km) has the second largest scale and Ar 013(3.0 km ×2.0 km) follows this, and both roughly extend in NW-SE direction. These zones occur in Cretaceous to Tertiary volcanic rocks.

(3) Lineaments

Regarding the distribution and directions of extracted lineaments in the area, some differences are observed between the northeastern margin and the western part.

(i) Northeastern margin

This part is mainly composed of Cretaceous to Tertiary volcanic rocks and sedimentary rocks, and NW-SE trending lineaments are generally predominant together with some NNE-SSW ones. Longest one trends in NW-SE direction with about 18 km long.

(ii) Western part

This part is underlain by Tertiary volcanic rocks, and lineaments in the part are densely concentrated. Most of lineaments are characterized by trending in NW-SE or NNW-SSE. Longest one has NNW-SSE trend and extends for 30 km.

Lineaments with NW-SE to NNW-SSE trends are recognized in the vicinity of alteration zones Ar 008, 009, 010, 013, 014 and 020.

(4) Fold structure and annular structure

(i) Fold structure

The structure was not interpreted in the area.

(ii) Annular structure

An annular structure is extracted and overlaps with one in SARAR DE SURIRE Area in the eastern vicinity of the area. The structure is inferred to be a crater wall of Tertiary-Quaternary volcano and is 5 km or more in diameter.

2-2-3 Salar de Surire sub-area

(1) Geologic units

The rocks and sediments in the sub-area are divided into six geologic units (shown in Plate 3 and Table 2-2-5). Of these units, one can be correlated with Cretaceous to Tertiary volcanic rocks, five with Tertiary to Quaternary volcanic rocks or sedimentary rocks, and five with Quaternary unconsolidated sediments. Moreover, one unit can be correlated to the intrusive body generated during Cretaceous to Tertiary time. Geologic unit K correlated with the Cretaceous volcanic rocks is distributed in NW-SE direction, and continuously extend into VOLCAN TACORA Area north of the area.

(2) Alteration zones

58 alteration zones (Alteration Zones SS 001 to 058) were extracted in the area (Plate 3 and Table 2-2-10). Among these, two altered zones (SS 001 and 002) overlap with VT 018, 019 of the VOLCAN TACORA Area north of the area , and 10 zones (SS 003, 004, 005, 006, 007, 008, 009, 010, 011 and 058) overlap with the zones (SS 007, 018, 011, 012, 013, 014, 015, 016, 017 and 020) of the ARICA Area near east of the area, respectively.

These zones are arranged in NW-SE direction in the northern and central parts. In the southern part, it is thought that altered zones arrange in NW-SE direction in the general situation though these are comparatively concentrated. The distribution density of the concentration part is very high. Each alteration zone generally shows an elliptic or an irregular amoeba form. The largest one of these zones is SS 007, which size is about 5.5 km $\times$3.5 km though it shows an irregular form. SS023, which has the second largest scale and forms slightly irregular, extends almost in NW-SE direction. Alteration zones which are larger scale such as SS 024,030,033 are observed around these.

These alteration zones are distributed in Cretaceous to Tertiary volcanic rocks in the northern and central parts, and occur in Tertiary to Quaternary volcanic rocks in the

southern part.

(3) Lineaments

Lineamants were extracted as shown in Plate 3 by the interpretation criteria explained in 2-1-4 (4).

Regarding the distribution and directions of extracted lineaments in the area, some differences are observed between the central to northern part and the southern part.

(i) Central to northern part

Volcanic rocks and unconsolidated sediments of Tertiary to Quaternary age are distributed in this area over the wide range except some Cretaceous to Tertiary volcanic rocks in the centeral to northern zones. NW-SE trending lineaments are predominant as a whole. Longest one reaches 30 km.

NW-SE trending lineaments are noted near the altered zones SS 001,002, and WNW-ESE or NW-SE trending ones are observed in the vicinity of altered zones such as SS 007, 008, 009, 057 and 058.

(ii) Southern part

This part is composed of Tertiary to Quaternary volcanic rocks, and lineaments are observed in high density.

In the southerncentral to southeastern zones of this part, NW-SE trending lineaments are intermittently developed in parallel at about 15 km intervals, and N-S or NNW-SSE trending lineaments intersecting to them are observed. NW-SE trending lineaments which run in parallel are intermittently developed for about 50 km. Most of lineaments are characterized by NW-SE or NNW-SSE trend. Longest one has NNW-SSE trend and extends for 30 km.

On the other hand, lineaments trending NE-SW are dominant together with some ENE-WSW ones in the western zone of the part. Most of those are about 5 km long though the one trending NE-SW is about 20 km long.

Lineaments with NW-SE and N-S trends are recognized in the vicinity of the altered zones such as SS 015, 016, 017, 018, 020, 022, 023, 024, 025, 026, 029, 030, 033, 034, 042 and 050.

(4) Fold structure and annular structure

(i) Fold structure

An anticlinal structure is interpreted in Cretaceous to Tertiary rocks distributed in the central part. The axis of the fold structure extends in NNW-SSE direction, and the structure plunges to the NNW.

(ii) Annular structure

Five annular structures are extracted. One of them overlaps with one in ARICA Area in the western vicinity of the area and is inferred to be caldera wall of Tertiary to Quaternary volcano. The annular structure in the central part is 7.5 km or more in diameter, and altered zones are dominant in and around the structure.

2-2-4 Mamiña sub-area

(1) Geologic units

The rocks and sediments in the sub-area are divided into 20 geologic units (shown in Plate 4 and Table 2-2-6). Of these, six units can be correlated with volcanic rocks and sedimentary rocks of Paleozoic to Cretaceous age, eight with Tertiary to Quaternary volcanic rocks or sedimentary rocks, and three with the unconsolidated sediments. Moreover, one geologic unit is correlated to Paleozoic plutonic rock or hypabyssal rock, and two can be correlated to the intrusive body generated during Jurassic to Tertiary time.

Geologic feature of this area is that Tertiary volcanic rock (geologic unit Tvs) occur widely in the central part and this rock is characterized by showing yellowish in false-color image. Moreover, Cenozoic unconsolidated sediments occur in the wertern part and Tertiary to Quaternary volcanic rocks are widely distributed in eastern part. In the false-color image, the latter is brown and shows rugged texture though the former is grayish brown and shows flowing texture.

(2) Alteration zones

63 alteration zones, which are Alteration Zones Ma 001 to 063, were extracted in this area (Plate 4 and Table 2-2-11). Among these, two zones (Ma 001 and 010) overlap with the zones SS 047 and 053 of SALAR DE SUNURE Area north of the area , and 8 zones (Ma 047, 048, 049, 050, 051, 053, 060 and 062) overlap with the zones (SL 001, 003, 004, 006, 005, 008, 002 and 009) of SALAR DELLAMARA Area south of the area, respectively. The zones are distributed dominantly in the northern and southern parts. These occur

scattered in the northern part and tend to be arranged in N-S direction. In the central part, alteration zones were hardly extracted in Tertiary volcanic rocks which is characteristic in yellowish in the false-color image. The zones generally show elliptic or irregular form. Ma 002 is the largest one of these zones and the size is about 7.0 km×2.0 km. Ma 055 (3.5 km ×3.0 km) has the next large scale by which Ma 040 (3.5 km×1.5 km)showing irregular form follows this. In addition, the zones such as Ma 020, 052, 053, 054 have comparatively large scale.

As for these alteration zones in the northern part, it is paid attention that about 12 zones are extracted in volcanic rocks (geologic unit Tv1) correlated to Tertiary to Quaternary time, though these occur mostly in Cretaceous volcanic rocks, Cretaceous to Tertiary volcanic rocks and granitic rocks. The alteration zones in the southern part are distributed in Jurassic sedimentary rocks, Cretaceous volcanic rocks, Cretaceous to Tertiary granite and Paleozoic volcanic rocks.

Alteration zone Ma 061 corresponds to Mocha mineral showings, Ma 031 to Cerro Colorado Mine, Ma 022 and 023 to Queen Elizabeth mineral showings, Ma 052 to Copaquire mineral showings and Ma 054 to Collaguasi Mine, respectively.

(3) Lineaments

Lineaments were extracted as shown in Plate 4 by the interpretation criteria explained in 2-1-4 (4).

Regarding the distribution and directions of extracted lineaments in the area, some differences are observed among the northern, central and southern parts.

(i) Northern part

This part is dominated by Cretaceous to Tertiary volcanic rocks and granitic rocks, and Tertiary to Quaternary volcanic rocks. In the eastern part of the area, the most continuous lineament is that changes its strike from NW-SE to NNW-SSE and runs consecutively in SALAR DE SURIRE Area, and its length reaches 40km. The other lineaments are less continuous and several km long excluding the one with about 10km long extracted in the cental part. Though lineaments with N-S trend are predominant in the central part, NW-SE and NE-SW trending ones are observed in the other parts.

NW-SE and NE-SW trending lineaments are recognized in the vicinity of altered zones Ma

002, 014, 024, 027, and Ma 008, 022, 063, respectively, and N-S trending ones are observed in the vicinity of Ma 019 and 023, additionally.

(ii) Central part

This part mainly consists of Tertiary volcanic rocks, and has the highest lineament density. Lineaments occur on the whole with a width of about 10km. The direction of dominant lineaments with N-S trend in the northern and southern zones changes into intesecting the N-S trend and NE-SW in the central zone. The distribution of lineaments is in reverse-S type as a whole. The lineaments with NE-SW trends intersecting the N-S system is characteristec of this part. Most continuous lineaments have N-S trend and reaches 40km long. In general, the continuity of NE-SW trending lineaments is poor.

(iii) Southern part

This part is chiefly composed of Paleozoic to Cretaceous volcanic and sedimentary rocks, and Tertiary to Quaternary volcanic rocks. In the whole area, lineaments are few in this part, and N-S trending ones are predominant. Though the lineaments in the southern zone occur with roughly N-S trend, the dominant lineaments in the central zone change the direction to NNW-SSE to the north, and intermittently extend for 45 km.

The altered zones Ma 037, 039 and 053 are extracted in the vicinity of N-S trending lineaments, and the zones Ma 038, 051 and 055 are observed in the vicinity of NW-SE trending ones.

(4) Fold structure and annular structure

(i) Fold structure

A syncline is interpreted in Jurssic and Cretaceous rocks in southern part of the area, and the axis of the structure extends in N-S direction.

(ii) Annular structure

Annular structure was not extracted in the area.

2-2-5 Salar de Llamara sub-area

(1) Geologic units

The rocks and sediments in the sub-area are divided into 17 geologic units (Plate 5 and Table 2-2-7). Of these units, five units can be correlated with Paleozoic to Cretaceous volcanic rocks and sedimentary rocks, six with Tertiary to Quaternary volcanic rocks or

sedimentary rocks, and three with the unconsolidated sediments. Moreover, one unit coresponds to Paleozoic plutonic or hypabyssal rock, and two can be correlated to the intrusive body generated during Jurassic to Tertiary time.

Geology of the area is characterized by Tertiary volcanic rocks (geologic unit Tvs) distributed widely in the central part. It has yellowish or grayish brown color in false-color image. Moreover, Cenozoic unconsolidated sediments are widely distributed in the wertern part, and Tertiary to Quaternary volcanic rocks are found widespread in eastern part. In the false-color image, the latter has brown color and shows rugged texture though the former is grayish brown and shows flow texture.

(2) Alteration zones

In the area, 36 alteration zones, named alteration zones SL 001 to 036, were extracted (shown in Plate 5 and Table 2-212). Among these, seven zones (Sl 001, 002, 003, 004, 005, 006 and 008) overlap with the zones Ma 047, 06, 048, 049, 051, 050 and 053 in MAMIÑA Area north of the area. The altered zones are observed in the central and eastern parts. These tend to concentrate in six places in the eastern part, and to be arranged in roughly N-S direction in the central part. The form of alteration zones generally is elliptic or irregular. The largest one of these zones is SL 004, which is equivarent to Ma 049, and the size is about 2.5 km×2.0 km. SL 014 with 3.5 km×2.0 km is the second largest one, and SL 008(equivarent to Ma 053) with 3.0 km×2.0 km extends in NW-SE direction.

The alteration zones in the eastern part are mostly distributed in Jurassic to Cretaceous volcanic rocks, and the zones in the central part dominantly occur in Jurassic volcanic and sedimentary rocks, Cretaceous volcanic rocks, and Paleozoic and Tertiary granitic rocks.

(3) Lineaments

Lineamants were interpreted as shown in Plate 5 by the interpretation criteria explained in 2-1-4(4).

Some differences are observed between the eastern and central parts regarding the distribution and directions of extracted lineaments in this area.

(i) Eastern part

This part is composed of Jurassic to Cretaceous volcanic rocks, Paleozoic to Cretaceous granitic rocks and Tertiary to Quaternary volcanic rocks. Generally, few lineaments are

recognized in this part. NNW-SSE and N-S trending lineaments are predominant, and lineaments with about 2-3 km length are dominant together with some 7-8 km ones.

NW-SE trending lineaments are observed in the vicinity of the altered zones SL 032 and 036.

(ii) Central part

The part consists of Paleozoic to Cretaceous volcanic and sedimentary rocks, and Tertiary volcanic rocks. In the whole area, lineaments in this part are distributed in high density. Though lineaments with N-S trend are predominant in the central part, ones with NE-SW trend tend to be dominant by facing to the west. N-S trending ones extend for 25 km, and run consecutively into MAMIÑA Area north of the part. Lineaments with NE-SW trend are discontinuous and about 10 km long.

Alteration zones SL 005, 014 and zones SL 008, 019, 021, 025, 026, 027, 028, 029 and zones SL 009, 015, 017, 018 are extracted in the vicinity of NW-SE, N-S and NE-SW trending lineaments, respectively.

(4) Fold structure and annular structure

(i) Fold structure

Bedding is interpreted clearly in Jurassic sedimentary rocks in the central part and fold structure is easily recognized in false-color images. Fold structures are extracted from six localities. These are three anticlines and three synclines and they occur repeatedly at 3-5 km intervals. The axis of fold structure extends roughly in the NNE-SSW direction.

(ii) Annular structure

Annular structure was not interpreted in this area.

2-2-6 Iquique sub-area

This sub-area lies within the overlap zone of the Arica and Mamiña sub-areas in the north and south respectively. Therefore, that of the above two images covers the interpretation of this sub-area.

Table 2-2-2 Photogeological Interpretation of TM Images

Area (Name of Image)	Number of Potogeologic Unit	Alteration Zone					Lineament					Folding / Annular Structure
		Number	Wall Rock Formation	Arrangement Direction	Shape (extension direction)	Size (km × km)	Number	Wall Rock Formation	Direction	Length (km)	Direction of Lineament near Alteration Z.	
VOLCAN TACORA	7 Cret. volc: 1 T-Q. volc: 3 Q. sed: 2 A: 1	20 duplicate; 3 (ARICA) 2 (SALAR D. S.)	Cret. volc.	NW-SE (2 rows)	elliptc, irregular (NNW-SSE～NNE-SSW, ENE-WSW)	max. 4 × 6.5	Northern: 7	Cret.-T. volc.	NW-SE, NNW-SSE	5～7	none	none
							Eastern: 6	Cret. volc, T-Q. volc	NW-SE, E-W	5～8	NW-SE	
							Western: 15	Cret. volc, Cret.-T. volc.	NW-SE, NNE-SSW	2～7	NW-SE, NNE-SSW	
ARICA	14 J. sed: 1 Cret.-T. volc: 2 T-Q. volc/sed: 5 Q. sed: 4 Cret.-T. int: 1 A: 1	20 duplicate; 3 (V. TACORA) 10 (SALAR D. S.)	Cret.-T. volc.	NNW-SSE～NW-SE	elliptc, irregular (NE-SW, NNW-SSE～N-S, WNW-ESE)	max. 4.5 × 2	Northeastern most: 4	Cret.-T. volc/sed	NW-SE, (NNE-SSW)	max. 18	none	1 annular str. : T-Q. crater rim (Φ 5km)
							Western: 95	T. volc.	NW-SE～NNW-SSE	max. 30	NW-SE, NNW-SSE	
SALAR DE SURIRE	13 Cret.-T. volc: 1 T-Q. volc/sed: 5 Q. sed: 5 Cret-T. int: 1 A: 1	58 duplicate; 2 (V. TACORA) 10 (ARICA) 2 (MAMIÑA)	Cret.-T(?). volc. T-Q. volc.	NNW-SSE	elliptc, irregular - amoebic (WNW-ESE, NNW-SSE～N-S, NW-SE, NE-SW)	max. 5.5 × 3.5	Central-Northern: 53	T-Q. volc/sed., (Cret.-T. volc)	NW-SE	max. 30	NW-SE, NNW-SSE, WNW-ESE	1 anticlinal str. with NNW-SSE axis, 5 annular strs. : T-Q. crater rim (max.Φ 7.5km) with Alt. Z.
							Southern: 117	T-Q. volc	NW-SE, N-S, NNW-SSE, NE-SW	5～30	WNW-ESE～NW-SE, NNW-SSE～NNE-SSW	
MAMIÑA	21 P-Cret. volc/sed: 6 T-Q. volc/sed: 8 Q. sed: 3 P. pluton/hypabyssal: 1 J-T. int: 2 A: 1	63 duplicate; 2 (SALAR D. S.) 8 (SALAR D. LL.)	Nortern: Cret-T. volc., Cret-T. gr., T-Q. volc.	Northern: N-S～sporadic	elliptc, irregular (NW-SE, NE-SW, NNW-SSE～NNE-SSW)	max. 7 × 2	Northern: 96	Cret-T. volc/gr, T-Q. volc.	N-S, NW-SE, NE-SW	max. 40	NW-SE, NE-SW, N-S～NNW-SSE	1 synclinal str. with N-S axis in J. & Cret.
							Central: 132	T. volc.	N-S, NE-SW	max. 40	N-S, NNW-SSE, NE-SW	
			Southern: P. volc., J. sed., Cret. volc., Cret-T. gr.	Southern: NNW-SSE			Southern: 47	P-Cret. volc/sed., T-Q. volc.	N-S	max. 45	N-S～NNE-SSW, NW-SE～NNW-SSE	
SALAR DE LLAMARA	18 P-Cret. volc/sed: 5 T-Q. volc/sed: 6 Q. sed: 3 P. pluton/hypabyssal: 1 J-T. int: 2	36 duplicate; 8 (MAMIÑA)	Eastern: J-Cret. volc.,	N-S	elliptc, irregular (E-W, NW-SE, N-S)	max. 2.5 × 2,	Eastern: 22	J-Cret. volc., P-Cret. Gr., T-Q.	NNW-SSE, N-S	2～8	NW-SE	3 anticlinal & 3 synclinal strs. with NNE-SSW axes in J. sed.
			Central: J. volc/sed., Cret. volc., P. gr., T. gr.				Central: 61	P-Cret. volc/sed., T. volc.	N-S, NE-SW	10～25	NNW-SSE～N-S, NNE-SSW	

Abbrev.
P=Paleozoic, J=Jurassic, Cret=Cretaceous, T=Tertiary, Q=Quaternary, A=Alteration, volc=volcanics, sed=sedimentary rock, int=intrusive, gr=granitic rock, str=structure, Alt. Z.=Alteration Zone

Table 2-2-3 Characteristics of Photogeologic Units of the VOLCAN TACORA Area

Unit	Photo-Characteristics		Mophologic Expression					Superficial Cover		Probable Lithology (Correlation with available Geologic Map)
	Tone	Texture	Drainage		Rock	Section	Bedding	Vegetation	Cultivation	
			Pattern	Density	Resistance					
Qd	gray, purplish gray	very fine	dichtomic	high	low		none	none	none	Unconsolidated sediments composed of talus deposits (Fluvial, Glacial, Alluvial, Mudflow)
TQ1	purplish red	very fine	sub-parallel	low	low		none	none	none	Unconsolidated sediments composed of gravel, sand, talus deposits(Pleistocene, Pliocene: Decitic ignimbrite,tuff, intercalated with continental sediments)
Tv3	brown	fine	radial	medium	high	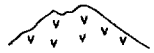	none	none	none	Volcanic rocks (Pliocene-Pleistocene : Andesite, basaltic flow, pyroclastic rocks)
Tv1	brown	fine	dendritic	medium	high	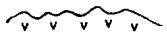	none	none	none	Volcanic rocks (Pliocene-Pleistocene : Andesite, basaltic flow, pyroclastic rocks)
Tvs	whitish yellow	very fine	dendritic	low	medium		none	none	none	Acidic Volcanic rocks (Plieocene-Miocene:Rhyolitic-basaltic flow, pyroclastic rocks, ignimbrite intercalated with continental sediments)
Jv	right brown	fine	dendritic	medium	high	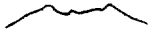	none	none	none	Volcanick rocks(Late-Middle Jurassic: Sandstone, calcareous sandstone)
K	brown	rough	dendritic	high	medium		none	none	none	Volcanic rocks (Early Tertiary-Late Cretaceous: Andesite-rhyolitic flow, pyroclastic rocks, dacitic-rhyolitic ignimbrite,)
A	light green	fine	none	low	low	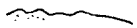	none	none	none	Alteration Zone (Hydrothermal alteration zone)

Table 2-2-4 Characteristics of Photogeologic Units of the ARICA Area

Unit	Photo-Characteristics		Mophologic Expression					Superficial Cover		Probable Lithology (Correlation with available Geologic Map)
	Tone	Texture	Drainage		Rock	Section	Bedding	Vegetation	Cultivation	
			Pattern	Density	Resistance					
Qa	gray	fine	meandering	very low	very low		none	none	none	Unconsolidated sediments composed of gravel, sand, silt and clay (Fluvial, Alluvial, Colluvial, Glacial, Lacustrine)
Qa1	purplish gray	very fine	parallel	high	low		none	none	partly	Unconsolidated sediments composed of gravel, sand, silt and clay,talus deposits (Fluvial, Alluvial, Colluvial)
Qd1	purplish brown	fine	parallel	medium	medium		none	none	none	Unconsolidated sediments composed of gravel, sand, silt clay and talus deposits (Fluvial, Alluvial, Colluvial)
TQ1	brown	fine ~ coarse	dendritec	medium	medium		none	none	none	Unconsolidated sediments composed of gravel ,sand, (Pleistocene-Pliocene: Decitic ignimbrite, tuff, intercalated with continental sediments)
Ts2	gray brownn	rough	parallel	very high	medium	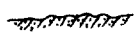	none	none	none	Fine to medium grained sedimentary rocks (Tertiary: Conglomerate, sandstone, mudstone)
Ts1	brown	fine	pinnate	very high	medium		none	none	none	Fine grained sedimentary rocks (Tertiary: Conglomerate, sandstone, mudstone)
Tv3	brown	fine	radial,	medium	high		none	none	none	Fine to medium grained sedimentary rocks (Tertiary: Conglomerate, sandstone, mudstone)
TV1	brown	fine	dendritic	high	high		none	none	none	Volcanic rocks (Pliocene-Pleistocene : Andesite, basaltic flow, pyroclastic rocks)
Tvs	yellow	coarse,rough	parallel	very high	high		none	none	none	Acidic Volcanic rocks (Plieocene-Miocene: Rhyolitic to basaltic flow and pyroclastic rocks, ignimbrite, intercalated with continental sediments)
K	brown	rough	dendritec	high	medium	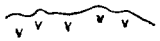	none	none	none	Volcanic rocks (Early Tertiary-Late Cretaceous: Andesite to rhyolitic flow and pyroclastic rocks, dacitic to rhyolitic ignimbrite,)
Kv	brown	rough	dendritic	high	medium	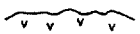	none	none	none	Volcanic rocks (Early Cretaceous : Andesite to rhyolitic / trachytic flows and pyrpclastic rocks, ignimbrite intecalated with sediments)
Jv	brown	rough	dendritic	low	medium	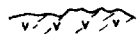	none	none	none	Volcanic rocks(Late-Middle Jurassic: andstone, calcareous sandstone)
Kg	brown	rough	dendritic	low	medium		none	none	none	Ineous rocks(Late Jurassic- Early Tertiary :Plutonic rocks)
A	right green	fine	none	none	low	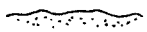	none	none	none	Alteratio Zone (Hydrothermal alteration zone)

Table 2-2-5 Characteristics of Photogeologic Units of the SALAR DE SURIRE Area

Unit	Photo-Characteristics		Mophologic Expression					Superficial Cover		Probable Lithology (Correlation with available Geologic Map)
	Tone	Texture	Drainage		Rock	Section	Bedding	Vegetation	Cultivation	
			Pattern	Density	Resistance					
Qa	brown	very fine	meandering	low	low		none	none	none	Unconsolidated sediments composed of gravel, sand, silt and clay (Fluviial, Glacial, Alluvial, Colluvial, Mud flow)
Qa1	gray,purplish gray	very fine	sub-parallel	high	low		none	none	none	Unconsolidated sediments composed of gravel, sand, silt and clay (Fluvial, Alluvial, Colluvial)
Qd	brown	fine	parallel	medium	low~medium	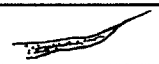	none	none	none	Unconsolideted sediments composed of talus deposits (Fluvial, Glacial, Alluvial, Mudflow)
Qd1	purplish brown	fine	sub-parallel	medium	medium		none	none	none	Unconsolidated sediments composed of gravel, sand, silt and clay (Pleistocene : Fluvial, talus deposits)
TQ1	brown	fine~rough	dendritic	medium	medium		none	none	none	Unconsolidated sediments composed of gravel, sand, (Pleistocene-Pliocene: Dacitic ignimbrite, tuff intercalated with continental sediments)
Ts2	gyay, brown	rough	parallel	very high	medium		none	none	none	Fine to medium grained sedimentary rocks (Tertiary: Conglomerate, sandstone ,mudstone)
Ts1	brown	fine	pinnate	very high	medium		none	none	none	Fine grained sedimentary rocks (Tertiary: Conglomerate, sandstone, mudstone)
Tv3	brown	fine	radial	medium	very high		none	none	none	Volcanic rocks (Pliocene-Pleistocene : Andesite, basaltic flow, pyroclastic rocks)
Tv1	gray, brown	fine~coarse	dendritic	high	medium ~high		none	none	none	Volcanic rocks (Pliocene-Pleistocene : Andesite, basaltic flow, pyroclastic rocks)
Tvs	yellow	coarse	dendritic	very high	high		none	none	none	Acidic Volcanic rocks(Plieocene-Miocene: Rhyolitic to basaltic flow and pyroclastic rocks, ignimbrite intercalated with continental sediments)
K	brown	rough	dendritic	high	medium		none	none	none	Volcanic rocks (Early Tertiary-Late Cretaceous: Andesite to rhyolitic flow and pyroclastic rocks, dacitic to rhyolitic ignimbrite)
Kv	light brown	rough	dendritic	high	medium	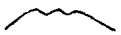	partly	none	none	Volcanic rocks (Early Cretaceous : Andesite to rhyolitic / trachytic flows and pyrpclastic rocks, ignimbrite intecalated with sediments)
Kg	brown	rough	dendritic	low	medium	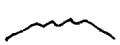	none	none	none	Ineous rocks(Late Jurassic- Early Tertiary : Plutonic rocks)
A	green, light green	fine	none	none	low		none	none	none	Alteration Zone (Hydrothermal alteration zone)

Table 2-2-6 Characteristics of Photogeologic Units of the MAMIÑA Area (1)

Unit	Photo-Characteristics		Mophologic Expression					Superficial Cover		Probable Lithology (Correlation with available Geologic Map)
	Tone	Texture	Drainage Pattern	Drainage Density	Rock Resistance	Section	Bedding	Vegetation	Cultivation	
Qa	gray	very fine	meandering, sub-parallel	very low	very low	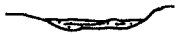	none	none	none	Unconsolidated sediments composed of gravel, sand, silt and clay (Fluvial, Glacial, Alluvial, Colluvial, Mud flow)
Qa1	gray	very fine	sub-parallel	high	low		none	none	none	Unconsolidated sediments composed of gravel, sand, silt and clay (Fluvial, Alluvial, Colluvial)
Qd	purplish gray	fine	parallel	medium	low~medium		none	none	none	Unconsolideted sediments composed of talus deposits (Fluvial, Glacial, Alluvial, Mudflow)
Ts3	brown	fine	dendritic	high	high		none	none	none	Fine to medium grained sedimentary rocks (Tertiary: Conglomerate, sandstone, mudstone)
Ts2	gray, brown	fine~rough	parallel	very high	medium	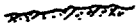	none	none	none	Fine to medium grained sedimentary rocks (Tertiary: Conglomerate, sandstone, mudstone)
Ts1	brown	fine	pinnate	very high	medium	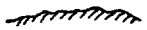	none	none	none	Fine grained sedimentary rocks (Tertiary: Conglomerate, sandstone, mudstone)
Ts	brown	fine	dendritic	low	medium		none	none	none	Coarse grained sedimentary rocks (Tertiary: Conglomerate, sandstone, mudstone)
Tv3	brown	fine	radial	medium	very high		none	none	none	Volcanic rocks (Pliocene-Pleistocene : Andesite, basaltic flow, pyroclastic rocks)
Tv2	brown	fine	radial	high	very high	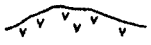	none	none	none	Volcanic rocks (Pliocene-Pleistocene : Andesite, basaltic flow, pyroclastic rocks)
Tv1	brown	fine	dendritic	high	medium~high	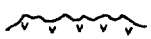	none	none	none	Volcanic rocks (Pliocene-Pleistocene : Andesite, basaltic flow, pyroclastic rocks)
Tvs2	dark gray	fine	sub-parallel	high	medium	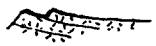	none	none	none	Unconsolidated sediments composed of gravel, sand, (Pleistocene-Pliocene : Dacitic ignimbrite, tuff, intercalated with continental sediments)
Tvs	yellow	fine	parallel	high	medium-high		none	none	none	Acidic Volcanic rocks(Plieocene-Miocene : Rhyolitic to basaltic flow and pyroclastic rocks ignimbrite, intercalated with continental sediments)
K	brown	rough	dendritic	high	medium	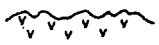	none	none	none	Volcanic rocks (Early Tertiary-Late Cretaceous: Andesite-rhyolitic flow, pyroclastic rocks, dacitic to rhyolitic ignimbrite)
Kv	light brown	rough	dendritic	high	medium		partly	none	none	Volcanic rocks (Early Cretaceous : Andesite to rhyolitic / trachytic flows and pyrpclastic rocks, ignimbrite, intecalated with sediments)
Js2	greenish brown	rough	dendritic	high	medium	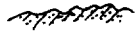	well bedded	none	none	Medium grained sedimentary rocks and Volcanic rocks (Late-Middle Jurassic: Sandstone, calcareous sandstone , limestone, marl, shale, conglomerate, chert)

Table 2-2-6 Characteristics of Photogeologic Units of the MAMIÑA Area (2)

Unit	Photo-Characteristics		Mophologic Expression					Superficial Cover		Probable Lithology (Correlation with available Geologic Map)
	Tone	Texture	Drainage Pattern	Drainage Density	Rock Resistance	Section	Bedding	Vegetation	Cultivation	
Js1	dark brown	rough	dendritic	high	medium	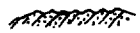	well bedded	none	none	Medium grained sedimentary rocks and Volcanic rocks (Late-Middle Jurassic: Sandstone, calcareous sandstone , limestone, marls, shale, conglomerate, chert)
Jv	right brown	fine	dendritic	medium	high		none	none	none	Volcanick rocks(Late-Middle Jurassic: Sand stone calcareous sandstone)
P	purplish brown	rough	dendritic	medium	medium		none	none	none	Volcanic rocks and Sedimentary rocks (Dacite , rhyolite, tuff, intercalated with sediments)
Ti	brown	rough	dendritic	medium	high		massive	partly	none	Igneous rocks (Terciary : Plutonic rocks and hypabyssal rocks)
Kg	brown	rough	dendritic	high	high		massive	none	none	Igneous rocks (Late Jurassic-EarlyTertiary : Plutonic rocks and hypabyssal rocks)
Pg	brownn	fine	dendritic	medium	high		massive	none	none	Igneous rocks (Paleozoic : Plutonic rocks and hypaby sal rocks)
A	green, light green	fine	none	none	low		none	none	none	Alteration Zone (Hydrothermal alteration zone)

Table 2-2-7 Characteristics of Photogeologic Units of the SALAR DE LLAMARA AREA (1)

Unit	Photo-Characteristics		Mophologic Expression					Superficial Cover		Probable Lithology (Correlation with available Geologic Map)
	Tone	Texture	Drainage		Rock	Section	Bedding	Vegetation	Cultivation	
			Pattern	Density	Resistance					
Qa	gray	fine	dichotomic	medium	low		none	none	none	Unconsolidated sediments composed of gravel, sand, silt and clay (Fluvial, Glacial, Alluvial, Colluvial, Mud flow)
Qa1	purplish gray	very fine	parallel	high	low		none	none	none	Unconsolidated sediments composed of gravel, sand, silt and clay(Fluvial, Alluvial, Colluvial)
Qd	gray,purplish gray	very fine	dichotomic	high	low		none	none	none	Unconsolideted sediments composed of talus deposits (Fluvial, Glacial, Alluvial, Mudflow)
Ts2	brown	fine	parallel	very high	medium		none	none	none	Fine to medium grained sedimentary rocks (Tertiary:Conglomerate, sandstone, mudstone)
Ts1	brown	fine	pinnate	very high	midium		none	none	none	Fine grained sedimentary rocks (Tertiary: Conglomerate, sandstone, mudstone)
Ts	brown	fine	dendritic	low	medium		none	none	none	Coarse grained sedimentary rocks (Tertiary: Conglomerate, sandstone, mudstone)
Tv3	dark brown	fine	radial	medium	high		none	none	none	Volcanic rocks (Pliocene-Pleistocene : Andesite, basaltic flow, pyroclastic rocks)
Tv1	brown	fine	dendritic	high	high		none	none	none	Volcanic rocks (Pliocene-Pleistocene : Andesite, basaltic flow, pyroclastic rocks)
Tvs	whitish yellow	very fine	dendritic	low	medium		none	none	none	Acidic Volcanic rocks(Plieocene-Miocene:Rhyolitic-basaltic flow , pyroclastic rocks, ignimbrite intercalation of continental sediments)
Kv	brown	rough	dendritic	high	medium		none	none	none	Sedimentary rocks (LowerJurassic: Marine and continental sedimentary rocks, Piltriquitron Formation etc.)
Js2	greenish brown	rough	dendritic	high	medium		well bedded	none	none	Medium grained sedimentary rocks and volcanic rocks (Late-Middle Jurassic: Sandstone, calcareous sandstone, limestone, marl, shale, conglomerate, chert)
Js1	dark brown	rough	dendritic	high	medium		well bedded	none	none	Medium grained sedimentary rocks and Volcanic rocks (Late-Middle Jurassic: Sandstone, calcareous sandstone, limestone, marl, shale, conglomerate, chert)
Jv	brown	fine	dendritic	medium	high		none	none	none	Volcanic rocks(Late-Middle Jurassic: Sandstone, calcareous sandstone)
P	purplish brown	rough	dendritic	medium	medium		none	none	none	Volcanic rocks and Sedimentary rocks (Dacite, rhyolite, tuff, intercalated with sediments)
Ti	brown	rough	dendritic	medium	high		massive	none	none	Igneous rocks (Tertiary : Plutonic rocks and hypabyssal rocks)

Table 2-2-7 Characteristics of Photogeologic Units of the SALAR DE LLAMARA AREA (2)

Unit	Photo-Characteristics		Mophologic Expression					Superficial Cover		Probable Lithology (Correlation with available Geologic Map)
	Tone	Texture	Drainage		Rock	Section	Bedding	Vegetation	Cultivation	
			Pattern	Density	Resistance					
Kg	brown	rough	dendritic	high	high		massive	none	none	Igneous rocks (Late Jurassic-EarlyTertiary : Plutonic rocks and hypabyssal rocks)
Pg	brown	fine	dendritic	medium	high		massive	none	none	Igneous rocks (Paleozoic : Plutonic rocks and hypabyssal rocks)
A	right green	fine	none	none	low	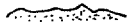	none	none	none	Alteration Zone (Hydrothermal alteration zone)

Table 2-2-8 Alteration Zones of the VOCAN TACORA Area

No. of Alteration	Nearby Units	Size (km)	Extension	Ore Deposit
VT001	K	(4+a)×6.5	NE-SW	
VT002	K	1.0×0.5	NW-SE	
VT003	K	7.5×1.8	NW-SE	
VT004	TQ1	1.0×1.0	—	
VT005	K	1.5×0.5	NE-SW	
VT006	K	1.5×0.7	N-S	
VT007	K	3.2×1.5	NNE-SSW	
VT008	K	2.2×1.5	N-S	
VT009	TV1	0.7×0.7	—	
VT010	K	1.5×0.7	NNW-SSE	
VT011	K	1.3×0.7	WNW-ESE	
VT012	K	1.0×0.7	NW-SE	
VT013	K	3.7×2.0	NE-SW	
VT014	K	1.5×0.7	NW-SE	
VT015	K	3.0×0.5	N-S	Same as Ar001
VT016	K	1.5×0.7	NE-SW	Same as Ar002
VT017	K	2.0×1.0	N-S	Same as Ar003
VT018	K	3.0×1.0	NNE-SSW	Same as SS001
VT019	K	1.5×1.0	NE-SW	Same as SS002
VT020	K	1.0×1.0	—	Same as Ar004

Table 2-2-9 Alteration Zones of the ARICA Area

No. of Alteration	Nearby Units	Size (km)	Extension	Ore Deposit
Ar001	K	3.0×0.5	N-S	Same as VT015
Ar002	K	1.5×0.7	NE-SW	Same as VT016
Ar003	K	2.0×1.0	N-S	
Ar004	K	1.0×1.0	—	Same as VT020
Ar005	K	1.0×1.0	—	
Ar006	K	2.0×1.5	NE-SW	
Ar007	K	4.5×2.0	NE-SW	Same as SS003
Ar008	K	2.0×0.5	—	
Ar009	K	1.5×1.0	—	
Ar010	K	2.0×0.7	N-S	
Ar011	K	2.5×1.7	NNW-SSE	Same as SS005
Ar012	K	1.5×1.0	NW-SE	Same as SS006
Ar013	K	3.0×2.0	NW-SE	Same as SS007
Ar014	K	3.5×2.0	NW-SE	Same as SS008
Ar015	K	2.0×0.5	WNW-ESE	Same as SS009
Ar016	Tv3	2.0×1.2	NW-SE	Same as SS010
Ar017	Tv3	1.0×0.7	NE-SW	Same as SS011
Ar018	Tv1	1.3×0.5	NW-SE	Same as SS004
Ar019	Kg	1.0×0.3	NW-SE	
Ar020	Tv3	0.7×0.2	NW-SE	Same as SS058

Table 2-2-10 Alteration Zones of the SALAR DE SURIRE Area

No. of Alteration	Nearby Units	Size (km)	Extension	Ore Deposit
SS001	K	3.0×1.0	NNE-SSW	Same as VT018
SS002	K	1.5×1.0	NE-SW	Same as VT019
SS003	K	2.0×4.5	NE-SW	Same as Ar007
SS004	Tv1	1.3×0.5	NW-SE	Same as Ar018
SS005	K	2.5×0.8	NNW-SSE	Same as Ar011
SS006	K	1.5×1.0	NW-SE	Same as Ar012
SS007	K	3.0×2.0	NW-SE	Same as Ar013
SS008	K	3.5×2.0	NW-SE	Same as Ar014
SS009	K	2.0×0.5	WNW-ESE	Same as Ar015
SS010	Tv3	2.0×1.2	NW-SE	Same as Ar016
SS011	Tv3	1.0×0.7	NE-SW	Same as Ar017
SS012	Tv1	0.7×0.3	NW-SE	
SS013	Tv1	4.5×1.5	NW-SE	
SS014	Tv1	1.5×1.2	NE-SW	
SS015	Tv1	3.5×1.0	NW-SE	
SS016	K	5.5×3.5	NW-SE	
SS017	K	1.5×1.0	N-S	
SS018	K	1.5×0.5	NW-SE	
SS019	K	2.0×1.0	NW-SE	
SS020	Tv1	1.5×0.7	N-S	
SS021	Tv1	1.5×0.7	N-S	
SS022	Tv1	2.5×1.0	NW-SE	
SS023	K	5.0×2.5	NW-SE	
SS024	K	3.0×3.0	–	
SS025	K	0.7×0.5	N-S	
SS026	Tv1	2.0×0.7	–	
SS027	K	1.0×0.7	–	
SS028	K	1.2×0.5	E-W	
SS029	K	2.3×0.5	E-W	
SS030	K	3.5×2.0	–	
SS031	Tv1	2.5×0.5	NNW-SSE	
SS032	Tv1	2.0×0.5	E-W	
SS033	Tv1	4.0×2.0	NW-SE	
SS034	Tv1	0.5×0.2	E-W	
SS035	Tv1	1.0×0.5	NE-SW	
SS036	Tv1	1.5×0.5	NW-SE	
SS037	Tv1	2.0×1.0	NW-SE	
SS038	Tv1	0.7×0.5	N-S	
SS039	Tv1	2.5×0.7	N-S	
SS040	Tv1	1.0×0.7	N-S	
SS041	Tv1	1.0×0.5	NW-SE	
SS042	Tv1	2.0×0.5	N-S	
SS043	Tv1	2.5×1.0	NE-SW	
SS044	Tv1	3.0×1.0	E-W	
SS045	Tv1	1.0×1.0	–	
SS046	Tv1	2.5×1.5	E-W	
SS047	Tv1	3.5×1.0	NE-SW	
SS048	Tv1	1.5×0.5	N-S	
SS049	Tv1	2.0×0.5	NW-SE	
SS050	K	0.5×0.5	–	
SS051	Tv1	0.7×0.7	–	
SS052	Tv1	0.8×0.5	N-S	
SS053	Tv1	1.0×0.7	N-S	
SS054	K	0.7×0.5	E-W	
SS055	K	1.3×1.0	E-W	
SS056	K	1.0×0.5	N-S	
SS057	K	1.5×0.7	N-S	
SS058	Tv3	1.0×0.3	NE-SW	Same as Ar020

Table 2-2-11 Alteration Zones of the MAMIÑA Area

No. of Alteration	Nearby Units	Size (km)	Extension	Ore Deposit
Ma001	Tv1	3.5×1.0	NE-SW	Same as SS047
Ma002	K	7.0×2.0	NW-SE	
Ma003	Tv1	0.5×0.3	NW-SE	
Ma004	Tv1	1.5×0.5	NE-SW	
Ma005	Tv1	2.0×1.0	NE-SW	
Ma006	Tv1	2.0×1.5	NMW-SSE	
Ma007	Tv1	2.0×1.2	NNE-SSW	
Ma008	Tv1	1.5×0.7	NW-SE	
Ma009	Tv1	1.7×1.0	NE-SW	
Ma010	Tv1	1.2×0.7	NE-SW	Same as SS053
Ma011	K	2.5×1.5	NME-SSW	
Ma012	Kv	1.5×1.0	NE-SW	
Ma013	Tv1	0.5×0.5	–	
Ma014	Kv	1.0×0.5	N-S	
Ma015	Kv	1.0×0.7	E-W	
Ma016	Kv	2.3×0.7	N-S	
Ma017	Tv1	1.0×0.5	NE-SW	
Ma018	Kg	2.5×1.5	NE-SW	
Ma019	Kg	2.0×1.0	NE-SW	
Ma020	Kv	2.0×2.0	–	
Ma021	Kv	1.0×0.5	N-S	
Ma022	Kg	1.0×0.7	NE-SW	Queen Elizabeth
Ma023	Kg	1.0×0.7	NW-SE	Queen Elizabeth
Ma024	Kv	1.0×0.5	N-S	
Ma025	Kv	1.7×0.5	NW-SE	
Ma026	Kv	1.0×0.7	NE-SW	
Ma027	Kv	0.7×0.7	–	
Ma028	Kv	1.2×0.7	E-W	
Ma029	Kv	1.5×1.0	–	
Ma030	Kv	1.5×1.0	E-W	
Ma031	Kv	1.5×1.0	NE-SW	Cerro Colorado
Ma032	Ts2	1.5×1.0	NE-SW	
Ma033	Tv1	1.7×0.5	NW-SE	
Ma034	J	1.5×1.0	N-S	
Ma035	Js1	1.3×1.0	NE-SW	
Ma036	Js1	0.7×0.5	N-S	
Ma037	Kv	2.0×1.0	N-S	
Ma038	Kv	1.5×0.8	NE-SW	
Ma039	Kv	2.5×0.8	N-S	
Ma040	Kv	3.5×1.5	–	
Ma041	Kv	1.5×0.7	NW-SE	
Ma042	Kv	1.0×0.7	NE-SW	
Ma043	Ti	0.7×0.5	NE-SW	
Ma044	Kv	1.0×0.7	–	
Ma045	Kv	0.7×0.6	E-W	
Ma046	Kv	2.0×1.0	NE-SW	
Ma047	Js2	2.0×1.0	NW-SE	Same as SL001
Ma048	Js2	1.5×0.7	NW-SE	Same as SL003
Ma049	Js2	2.5×2.0	–	Same as SL004
Ma050	Js2	1.8×0.7	NW-SE	Same as SL006
Ma051	Ti	3.0×0.3	NNW-SSE	Same as SL005
Ma052	Js2	3.2×1.5	NE-SW	Copquire
Ma053	P	3.5×1.5	E-W	Same as SL008
Ma054	P	3.0×0.7	E-W	Collaguasi
Ma055	P,Pg	3.5×3.0	–	
Ma056	P	1.5×0.5	NE-SW	
Ma057	Tv1	1.0×0.5	NW-SE	
Ma058	P	0.7×0.5	NW-SE	
Ma059	P	1.0×0.5	E-W	
Ma060	Js2	1.5×0.7	N-S	Same as SL002
Ma061	Kv	1.3×1.0	N-S	Mocha
Ma062	Ts	1.0×0.7	NW-SE	Same as SL009
Ma063	Kg	1.7×0.5	–	

Table 2-2-12 Alteration Zones of the SALAR DE LLAMARA Area

No. of Alteration	Nearby Units	Size (km)	Extension	Ore Deposit
SL001	Js2	2.0×1.0	NW-SE	Same as Ma047
SL002	Js2	1.5×0.7	N-S	Same as Ma060
SL003	Js2	1.5×0.7	NW-SE	Same as Ma048
SL004	Js2	2.5×2.0	—	Same as Ma049
SL005	Ti	3.0×0.3	NNW-SSE	Same as Ma051
SL006	Js2	1.8×0.7	NW-SE	Same as Ma050
SL007	Js2	2.0×1.0	NW-SE	
SL008	P	3.0×0.7	E-W	Same as Ma053
SL009	Ts	1.0×0.7	NW-SE	
SL010	Js2,Ti	2.0×2.0	—	
SL011	Js2	0.7×0.5	NE-SW	
SL012	Js2	0.3×0.2	E-W	
SL013	Js2	1.0×0.5	NE-SW	
SL014	Js2,Ti	2.5×1.5	N-S	
SL015	J	0.5×0.3	N-S	
SL016	Js1	0.7×0.5	N-S	
SL017	Pg	0.7×0.5	N-S	
SL018	Pg	0.7×0.5	NW-SE	
SL019	Ti	1.5×0.7	N-S	
SL020	Js1	1.0×0.3	N-S	
SL021	Js1	1.7×0.7	N-S	
SL022	Qa	1.0×0.3	NW-SE	
SL023	Js1	0.5×0.3	NE-SW	
SL024	J	0.6×0.3	NW-SE	
SL025	Ti	0.7×0.3	NW-SE	
SL026	Js1	1.5×0.3	N-S	
SL027	Js1	0.5×0.3	NW-SE	
SL028	Js1	0.7×0.5	NE-SW	
SL029	Js1	0.7×0.5	NE-SW	
SL030	Js1	0.5×0.3	NW-SE	
SL031	Kv	1.5×1.0	E-W	
SL032	Jv	0.7×0.5	NW-SE	
SL033	Kv	1.5×0.5	E-W	
SL034	Kv	1.5×1.5	—	
SL035	Jv	1.5×0.5	NW-SE	
SL036	Jv	1.0×0.5	NW-SE	

70° W

69° W

N

W

E

S

PERU

18° S

BOLIVIA

19° S

20° S

Legend

Annular structure

Fold

anticline

syncline

Lineament

certain

uncertain

Photogeologic Unit from TM images

Lake

alteration zone (A)

Unconsolidated sediments (Qa)

Unconsolidated sediments (Qa1)

Unconsolidated talus deposits (Qd)

Unconsolidated sediments (Qd1)

Fine to medium-grained sediments (Ts3)

Fine to medium-grained sediments (Ts2)

Unconsolidated sediments, dacitic ignimbrite (TQ1)

Unconsolidated talus deposits (Tvs2)

Volcanic rocks (Tv3)

Volcanic rocks (Tv2)

Volcanic rocks (Tv1)

Acidic volcanic rocks (Tvs)

Fine-grained sediments (Ts1)

Fine to medium-grained sediments (Ts)

Volcanic rocks (K)

Volcanic rocks (Kv)

Medium-grained sedimentary rocks and volcanic rocks (Js2)

Medium-grained sedimentary rocks and volcanic rocks (Js1)

Volcanic rocks (Jv)

Volcanic rocks and sedimentary rocks (P)

Intrusive Rocks

Igneous rocks (Ti)

Igneous rocks (Kg)

Igneous rocks (Pg)

0 50 100 km

Fig. 2-2-2 Photogeologic Interpretation Map of TM images

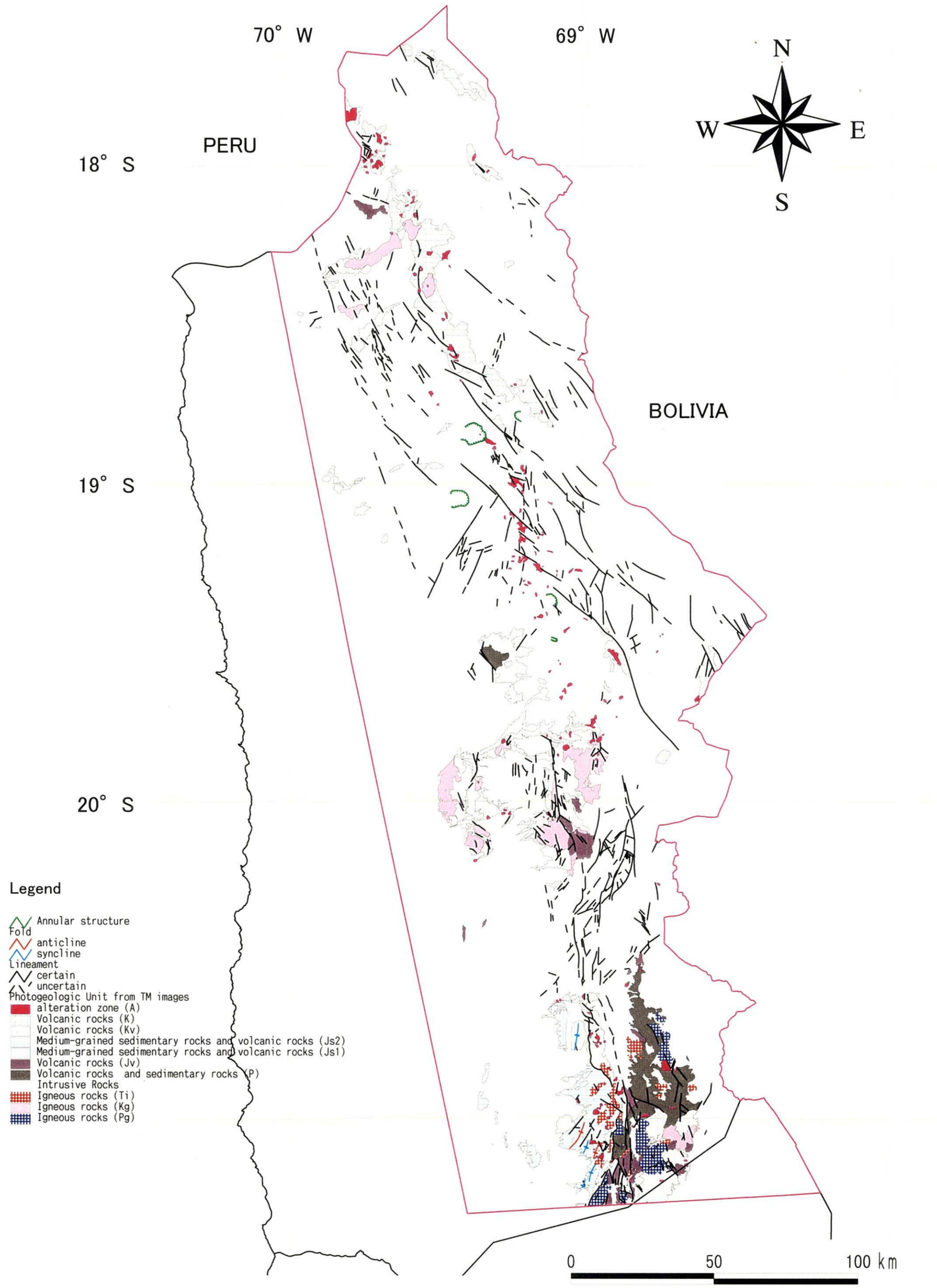

Fig. 2-2-3 Photogeological Structure of the Study Area

CHAPTER 3 GEOLOGICAL SURVEY AND GEOCHEMICAL SURVEY

When relatively large areas (100km^2 or larger) are selected for geological and geochemical surveys, mineral prospects extracted by examination of existing documents and alteration zones extracted by satellite image analysis are regionally expressed only as distribution of dots. Therefore, we believe that vicinity of the mineral prospects and alteration zones should also be included in target areas for extracting areas with high mineral potential. Large porphyry copper deposits (Cerro Colorado, Collaguasi) do not necessarily coincide with alteration zones extracted from images. Also lineament and fault zones and occurrence of ore deposits are considered to be closely related. But the large porphyry copper type deposits occur at the central or peripheral parts of fractured zones, and thus promising mineral zones cannot be selected from fracture zone – ore-deposit distribution relationship.

From the above reasoning and consideration of the distance between mineral prospects and alteration zones, it was thought that area within 4km radius from mineral prospects and alteration zones would be the mineral high-potential areas. The promising areas finally selected for porphyry copper deposits consist of high potential zones including Cu, Mo, and Au prospects and areas where high potential zones including alteration zones overlap (Fig. 2-3-1).

Reconnaissance survey was carried out in parts of the above promising areas for ore-deposit occurrence and known porphyry copper prospects with the purpose of verifying geologic structure, mineralization, and alteration zones and samples were collected. The areas of this ground survey are shown in Figure 2-3-2. Laboratory examination carried out on the collected samples is shown in Table 1-1.

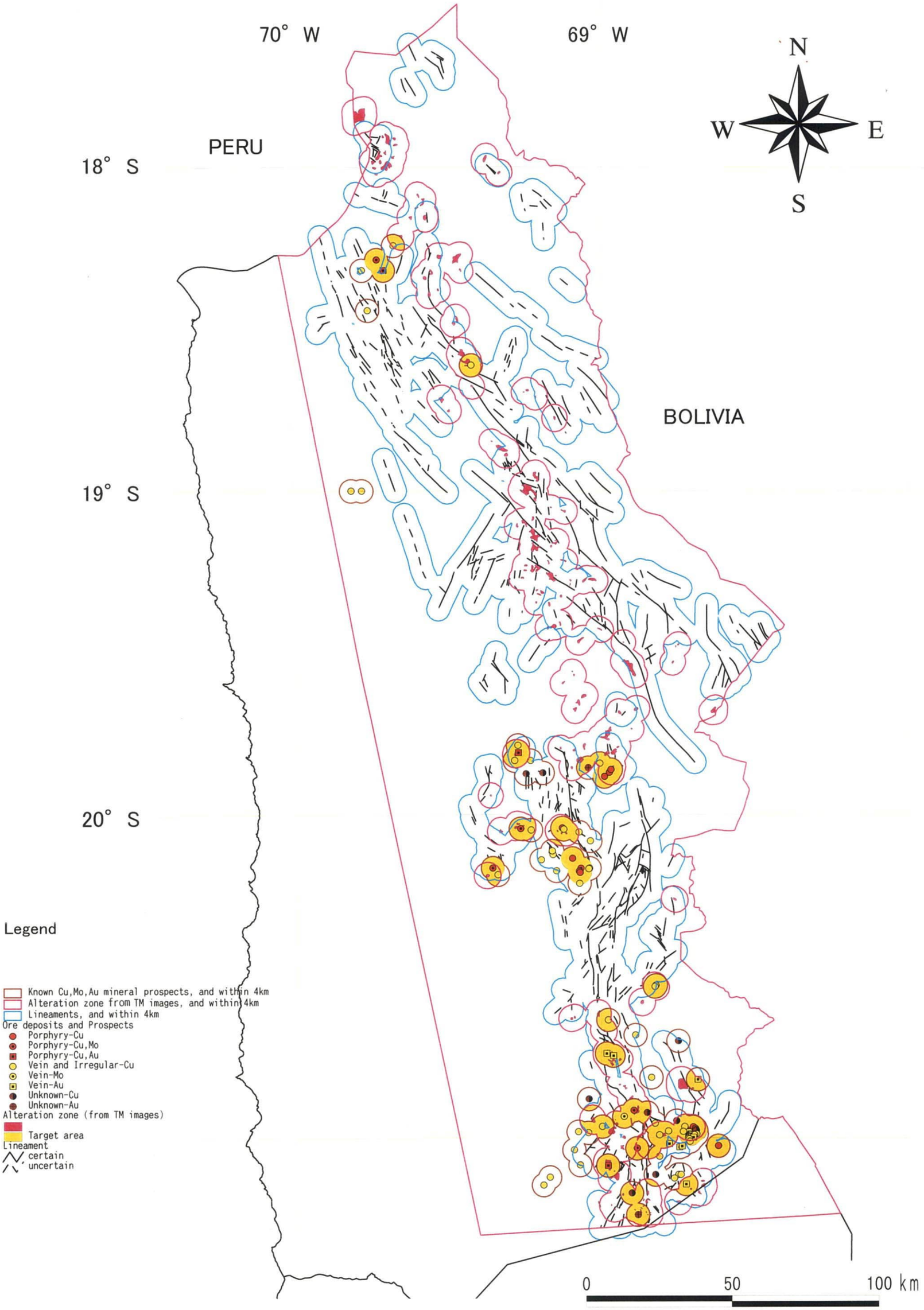

Fig. 2-3-1 Target Areas Plotted from Analysis of Satellite Images and Existing Data

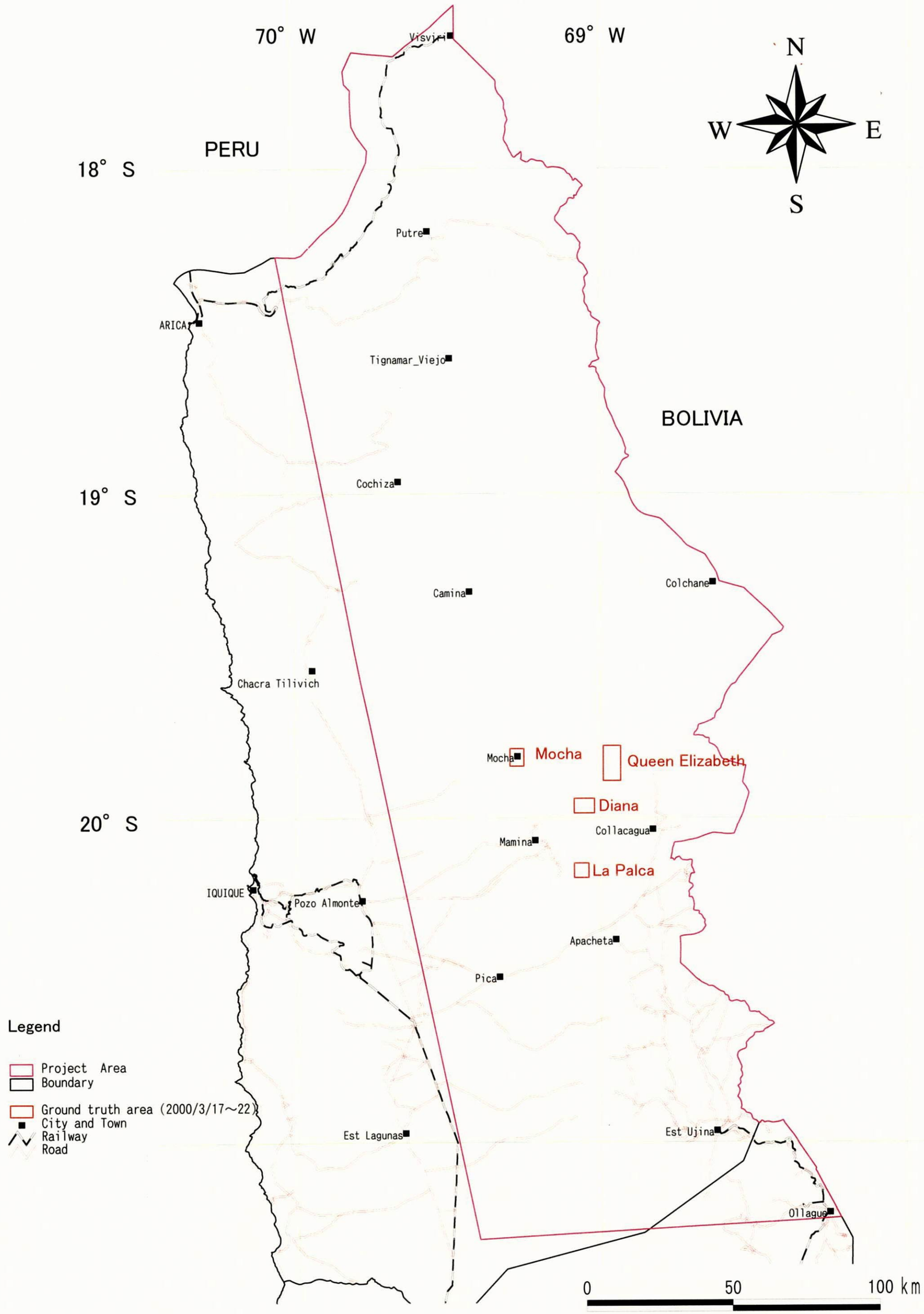

Fig. 2-3-2 Location Map of the Ground Truth Area

PART III CONCLUSIONS AND RECOMMENDATIONS

PART III CONCLUSIONS AND RECOMMENDATIONS

CHAPTER 1 CONCLUSIONS

Analysis of existing data including GEOSCAN image analysis, satellite image analysis, and geological survey and geochemical survey were carried out in Region I during the first year survey and the following conclusions were reached.

1. Many alteration zones were extracted in Paleogene and older formation and vicinity and in Miocene-Quaternary volcanic rocks by TM image analysis. These alteration zones are aligned in the NW-SE~NNW-SSE direction in the northern part, and in N-S~NNW-SSE direction in the central to the southern parts of the survey area. The above direction of alteration zone alignment is harmonious with the prominent direction of the lineaments developed in the alteration zones.

2. Analysis of images of visible near infrared-short-wave infrared region, short-wave infrared region, and thermal infrared region was carried out and the following results were obtained. Detailed geologic structure was clarified; alteration zones consisting of sericite, kaolin, alunite, and silica were extracted at Tignamar, Palca, Queen Elizabeth, Cerro Colorado, Copaquiri, and Collahuasi areas; and sericitized zone was extracted at Mocha area.

3. Mineralization of the known deposits and mineral prospects of the survey area was classified from the analysis of existing data on geology and ore deposits. And porphyry copper-type mineralized zones and possibly closely related prospects (Mo veins, irregular Cu, Cu veins, unknown-shaped Cu, Au veins, unknown-shaped Au) were selected.

4. Many mineral prospects closely related to porphyry copper-type mineralized zones are distributed in Paleocene-early Eocene porphyry copper belt in the northern part, and in Paleocene-early Eocene and late Eocene-early Oligocene porphyry copper belts in the central to southern parts of the survey area. Epithermal mineralized zones related to Miocene-Quaternary igneous activity occur in the northern to central parts of the area and some of it is believed to overlap with the porphyry copper mineralized zones.

5. Porphyry copper mineralized zones and possibly closely related prospects occur in and near Cretaceous-Tertiary intrusive bodies (plutonic and hypabyssal rocks).

6. Porphyry copper mineralized zones occur; in the northern and central parts in Cretaceous-Tertiary intrusive bodies or in Cretaceous volcanic rocks, and in the southern part in Paleozoic sedimentary and volcanic rocks, Cretaceous volcanic rocks, Paleozoic granitic rocks, or in Cretaceous-Tertiary intrusive bodies.

7. Faults on geological maps and fractures expressed as lineaments extracted from TM images are fractures which are generally closely related to the occurrence of ore deposits and prospects. The direction of the lineaments near the deposits and prospects is diverse. The porphyry copper mineralized zones occur either in the peripheries of the zones where lineaments are developed (Cerro Colorado, Collahuassi, etc.,) or near the center of lineament concentration (Quebrada Blanca, Copaquire, etc.).

8. In the central and southern parts many mineral prospects including porphyry copper mineralized zones occur in the alteration zones or vicinity, while in the northern part many of them occur in localities where alteration zones have not been extracted.

9. Assuming that hydrothermal activity related to mineralization is effective within a range of 4km from the alteration zones and ore deposits and prospects, hydrothermal zones are generally elongated in the NNW-SSE direction, but existence of those elongated in the E-W direction intersecting the major NNW-SSE direction is inferred. The known porphyry copper mineralized zones occur in this E-W hydrothermal system. The hydrothermal zones coincide with lineament concentration in the central and southern parts, but the correlation between the two is relatively poor in the northern part, with better coincidence with the distribution of Miocene-Quaternary volcanoes.

10. The following localities were selected as promising for porphyry copper occurrence.
Porphyry copper-type mineral prospects and within 4km range.
Mineral prospects possibly related to porphyry copper mineralization in Oligocene and older formations (Mo veins, irregular Cu, Cu veins, unknown-shaped Cu, Au veins, unknown-shaped Au) and alteration zones (acidic alteration zones and sericitized zones extracted by GEOSCAN image analysis and alteration zones

extracted by TM image analysis), and within 4km of the above.

CHAPTER 2 RECOMMENDATIONS FOR THE SECOND YEAR SURVEY

1. It is recommended that verification survey be carried out in localities selected as promising for porphyry copper occurrence and were not surveyed during the first year.

2. Geomagnetic anomalies at right angles to the axis of Central Andes are probably closely related porphyry copper-type mineralized zones. The existing airborne geomagnetic maps are not sufficiently precise for extracting promising zones. Therefore, it is recommended that high precision airborne geomagnetic survey be carried out and the details of the above trans-Central Andes geomagnetic anomalies be clarified. This will result in more focused targeting of the promising localities and in selection of promising localities for blind buried deposits in areas where alteration zones were not detected because of coverage by younger formations.

3. It is recommended that gravity survey be carried out in localities extracted as promising for porphyry copper occurrence by the above high precision airborne geomagnetic survey so that the thickness of the formations overlying mineralized zones can be inferred.

4. It is recommended that geological reconnaissance be carried out in localities considered to be promising from the results of image analysis and high precision airborne geomagnetic survey.

Reference

Clark, A. H., Archibald, D. A., Lee, A. W., Farrar, E., and Hodgson, C. J., 1998. Laser Probe $^{40}Ar/^{39}Ar$ Ages of Early- and Late-stage Alteration assemblages, Rosario Porphyry Copper-Molybdenum deposit, Collahuasi District, I Region, Chile, Econ. Geol., 93, p.326-337.

Davidson, J., and Mpodozis, C., 1991. Regional Geologic Setting of Epithermal Gold Deposits, Chile, Econ. Geol., 86, p.1174-1186.

Kahle, A. B., and Goetz, A. F. H., 1983 : Mineralogic Information from a New Airborne Thermal Infrared Multispectral Scanner, Science, vol. 222, p.24-27.

Mpodozis, C., and Ramos, V., 1989. The Andes of Chile and Argentina, Geology of the Andes and its relation to hydrocarbon and mineral resources: Circum-Pacific Council for Energy and Mineral Resources Earth Science Series, vol. 11, p.59-89.

Metal Mining Agency of Japan, 1978. Overseas Geologic Structure Survey Report: Northern Chile

Metal Mining Agency of Japan, 2000. Research and Development on Satellite Data Analysis

Olivier, C. G., and Dingman, R. J., 1962. Carta Geologica de Chile, Cuadrangulos Pica, Alca, Matilla y Chacarilla, Provincia de Tarapaca, Escala 1:50,000, Institute de Investigaciones Geologicas, Chile, vol.III No.2, 3, 4 y 5.

Olivier, C. G., 1968. Carta Geologica de Chile, Cuadrangulo Juan de Morales, Provincia de Tarapaca, Escala 1:50,000, Institute de Investigaciones Geologicas, Chile, Carta No.18.

Ramirez, C.,F.,R., and Huete, C. L.,1981. Carta Geologica de Chile, Escala 1:250,000, Hoja Ollague Region de Antofagasta, Institute de Investigaciones Geologicas, Chile, Carta No.40.

Salas, R. O., Kast, R. F., Montecinos, F. P. and Salas, I. Y., 1966. Geologia y recursos minerales del departamento de Arica, Provincia de Tarapaca, Institute de Investigaciones Geologicas, Chile, Boletin No.21.

Sillitoe, R. H., 1991. Gold Metallogeny of Chile –an Introduction, Econ. Geol., 36, p.1187-1205.

Sillitoe, R. H., 1992. Gold and Copper Metallogeny of the Central Andes-Past, Present, and Future Exploration Objectives, Econ. Geol., 87, p.2205-2216.

Skarmeta, J. M., and Marinobic, N. S., 1981. Carta Geologica de Chile, Escala 1:250,000, Hoja Quillagua Region de Antofagasta, Institute de Investigaciones Geologicas, Chile, Carta No.51.

Thomas, A. N., 1967. Carta Geologica de Chile, Cuadrangulo Mamiña, Provincia de Tarapaca, Escala 1:50,000, Institute de Investigaciones Geologicas, Chile, Carta

No.17.

Vergara, H. L.,and Thomas A.N., 1984. Carta Geologica de Chile, Escala 1:250,000, Hoja Collacagua, Region de Antofagasta, Servicio Nacional de Geologia y Mineria, Chile, Carta No.59.

Yamaguchi, Y., Urai, M., Honey, F. A., 1989. Distinguishing Lithology by Spectral Characteristics – An example in Australia by Geoscan AMSS MkI – Jour. JPN Remote Sensing Society, vol.9, no.3, 19-29.